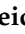


Article

Numerical Study on Optimal Scheme of the Geothermally Heated Bridge Deck System

Weidong Lyu ¹, Hefu Pu ^{1,*}, Jiannan (Nick) Chen ^{2,*} and Zelei Gao ³

¹ School of Civil and Hydraulic Engineering, Huazhong University of Science and Technology, Wuhan 430074, China; weidonglyu@hust.edu.cn

² Department of Civil, Environmental, and Construction Engineering, University of Central Florida, Orlando, FL 32816, USA

³ College of Civil Engineering and Architecture, Zhejiang University, Hangzhou 310058, China; 11912030@zju.edu.cn

* Correspondence: puh@hust.edu.cn (H.P.); jiannan.chen@ucf.edu (J.C.); Tel.: +86-1777-186-8369 (H.P.)

Received: 26 October 2020; Accepted: 14 December 2020; Published: 16 December 2020



Abstract: Ground source deicing system application in bridge decks is an alternative to salt use, which reduces corrosion and extends the deck service life. Herein, a preliminary parametric numerical analysis is performed to investigate the effects of several important parameters (tube spacing, inlet temperature, flow rate, and concrete cover) on heat transfer performance. Three evaluation indexes (average top surface temperature, snow melting proportion, and heat absorption power) are introduced, and a synthetic evaluation index is proposed to comprehensively consider factors. Mainly referring to the synthetic evaluation index, the optimal design scheme of a geothermally heated bridge deck system under various conditions (layout, lane number, ambient temperature, and tube spacing) is obtained and analyzed to determine the optimal inlet temperature and guide heated bridge deck design. Finally, the influence of wind speed and two adjustment methods are studied. The results indicate that the horizontal layout is the recommended circulating tube layout. The established empirical equations reveal that the optimal inlet temperature is linearly related to ambient temperature and exhibits a quadratic relationship with tube spacing. There is no need to add a heat insulation layer at the bridge deck bottom, and only tubes arranged near the wheels in lanes are recommended.

Keywords: geothermal energy; deicing system; bridge decks; evaluation indexes; optimal design scheme

1. Introduction

In the cold winter, when road surfaces become icy due to snowfall, road surface adhesion is greatly reduced, which affects the dynamics and safety of driving. Ice often causes brake failures, and frequent traffic accidents and continuous rear-end collisions are common. The efficiency of road transportation on icy and snowy days is extremely low. Traffic accidents not only threaten the lives of drivers and passengers but also cause serious damage to transportation facilities and vehicles and may even result in road closure, which causes inconvenience to passenger and cargo transportation [1].

Typical snow removal methods currently applied include the mechanical removal method, chemical treatment method, and electric heating method [2,3]. However, these methods have certain disadvantages. Some methods are inefficient, while some are uneconomical. For example, mechanical removal simply plows snow to the road sides but does not truly eliminate snow. Mechanical removal is mainly suitable for snow removal on heavy snow days, and this method is a passive operation with hysteresis characteristics. The application of salt and other chemicals does not melt snow when

the temperature falls below $-3.9\text{ }^{\circ}\text{C}$ [4]. Moreover, this method may lead to concrete corrosion and bridge deck service life reduction [5,6]. Electric heating has also been employed to melt snow [7]. Maleki et al. [8] investigated an electrically conductive concrete slab. Liu et al. [9] presented a method of melting snow with carbon fiber heating wires buried in cement concrete pavement. Liu et al. [10] proposed two thermal field prediction models of ice-snow melting pavement. Lai et al. [11] presented a method of melting ice with carbon fiber heating wire buried in concrete pavement to avoid the adverse effects of snow melting chemicals. Overall, the method of electric heating responds fairly quickly to snowfall, but it is expensive to install and maintain. In addition, it consumes large amounts of either electricity or fuel, which emits additional CO_2 [12,13].

Due to global climate change, many researchers have increasingly focused on renewable energy sources, e.g., wind, solar, and geothermal energy. Wang et al. [14] performed dynamic snow melting experiments on a hydronic-heated inclined pavement. Spittler et al. [15] described a simulation methodology of bridge deck deicing systems that utilize a ground source heat pump system. Ho et al. [16] studied a piped hydronic pavement heating system. Yehia et al. [17] used the conductive concrete overlay method. Chen et al. [18] investigated the snow melting process on asphalt pavements by experiments and numerical simulation. Pan et al. [19] summarized the major achievements of existing literatures regarding hydronic asphalt pavement. Since environmental issues are serious, we must consider the environmental impact of snow melting methods. Geothermal energy may be a good alternative to melt snow because it uses less fuel energy than do electric heating systems. Based on the above reasons, many researchers have analyzed geothermally heated systems. Liu et al. [20] conducted simulation of hydronic snow melting systems for bridges. A simple snow melting system was simulated by Liu et al. [21] to evaluate the performance of a bridge under realistic transient operating conditions. Wang and Chen [22] presented a theoretical model describing the heat and mass transfer processes during the melting of snow on pavement. Olgun et al. [23] presented a summary of thermo-active geotechnical systems for near surface geothermal energy. Bower et al. [24] outlined the operational principles and how these are related to the design parameters of bridge deck deicing systems. Chiasson et al. [25] described a design and simulation tool for modeling the performance of a hydronic pavement heating system as a supplemental heat rejecter in ground-source heat pump systems.

Moreover, some researchers focused on the relation with natural groundwater flow and heat. Maya et al. [26] presented novel advances in the upscaling of operation datasets obtained from open-loop geothermal energy systems for an optimal integration in hydrogeological models. García-Gil et al. investigated two real groundwater heat pump systems using real exploitation data sets to estimate the thermal energy demand bias and to assess the nature of thermal interferences between the systems [27] and defined the exploitation patterns of groundwater heat pump systems [28].

Operating condition-dependent design is one of the important design aspects of a geothermal snow melting system. Because of the deficiencies in previous research in terms of geothermal snow melting system design, the current study examines optimization methods in detail. First, a geothermally heated bridge deck is introduced as an example to study geothermally heated systems. Second, a preliminary parametric numerical analysis is performed to investigate the effects of several important parameters (i.e., tube spacing, inlet temperature, flow rate, and concrete cover) on the heat transfer performance. Third, three evaluation indexes (i.e., average top surface temperature, snow melting proportion, and heat absorption power) are introduced, and a synthetic evaluation index is then defined and proposed to comprehensively consider the influencing factors. Mainly based on the proposed synthetic evaluation index, the optimal design scheme of a geothermally heated bridge deck system under various conditions (i.e., tube layout, lane number, ambient temperature, and tube spacing) is studied to determine the optimal inlet temperature and to guide heated bridge deck design. Finally, the influence of the wind speed and two adjustment methods (i.e., the addition of a heat insulation layer at the bottom of the bridge deck and only arranging tubes near wheels) is studied.

2. Materials and Methods

2.1. Geothermally Heated Bridge Deck System

A configuration of a geothermally heated bridge deck system is shown in Figure 1 [29]. In this figure, both the heat exchangers in the deep foundations and shallow heat exchangers in the embankments extract thermal energy from the ground to regulate the bridge deck temperature. The whole system is divided into four parts: heated bridge deck system, ground source heat pump system, energy foundation system, and automatic control system.

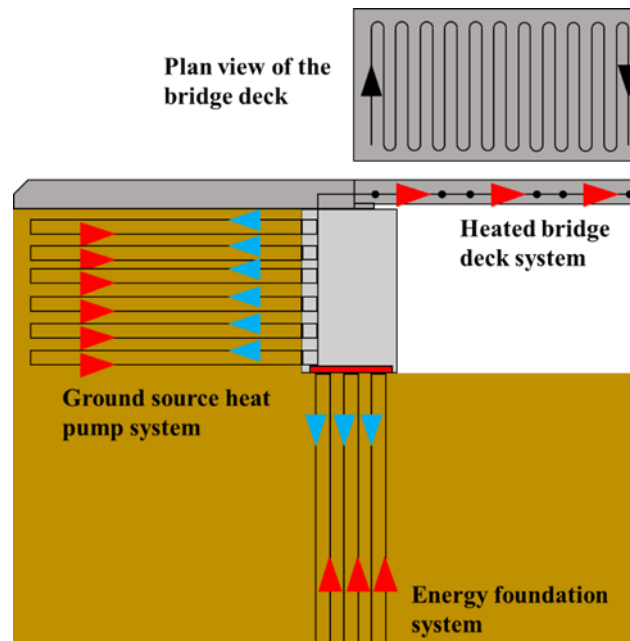


Figure 1. Example of the geothermal heat exchangers used for bridge deck deicing (adapted from Bowers et al. [29]).

The heated bridge deck system, as shown in Figure 2, is a heated bridge deck with embedded circulating tubes. Heat transfer fluid (typically water) is circulated in the tubes. Heat is transferred to the bridge deck through the tube walls. The ground source heat pump system consists of loops embedded in the embankment. The energy foundation system (typically consisting of energy piles) comprises loops embedded in the energy foundation. Both the ground source heat pump system and energy foundation system extract thermal energy from the ground, which is employed to regulate the bridge deck temperature. To effectively and reliably prevent icing and to achieve deicing with minimal energy consumption, the operation of the whole system should be controlled by an automatic control system. All ice melts as long as the ice and snow on the concrete surface reach a temperature above zero. When the system is operated in real time, the concrete surface temperature ranges from 2~3 °C, and the deicing effect is the best. We can control the temperature of the bridge deck within this range through the automatic control system. First, according to meteorological forecasts, the preheating time is estimated based on the air temperature and wind speed during snowfall, and the heated system is activated in advance to preheat the bridge deck so that no snow accumulates on the road surface during snowfall. The surface temperature of the bridge panel is monitored in real time. When the temperature is higher than 3 °C, heating is stopped. In contrast, at a temperature below 2 °C, heating is initiated.

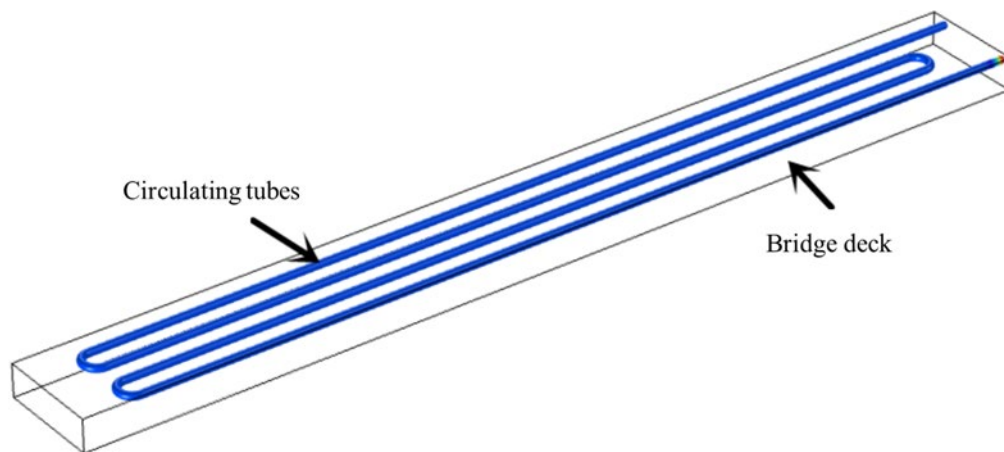


Figure 2. Schematic of the heated bridge deck system.

2.2. The Heated Bridge Deck Numerical Model

The research emphasis of this study is to analyze the heat transfer process of the bridge deck under the influence of heat transfer fluid circulation in the circulating tubes. In this study, the heated bridge deck system is numerically simulated with commercial software COMSOL Multiphysics 5.3 [30]. Three physical modules (i.e., the solid heat transfer module, fluid heat transfer module, and nonisothermal pipe flow module) are employed. The solid heat transfer module is adopted to simulate the conduction and heat radiation in the solid. The fluid heat transfer module is applied to simulate the heat conduction and heat convection in the airflow or fluid flow. The nonisothermal pipe flow module is used to calculate the temperature, velocity, and pressure of the fluid field. This module adopts a one-dimensional curve or straight line to represent the flow in the tube section by setting the inner diameter and wall thickness of the hollow tube to achieve simulation simplification. This is a study based on numerical evaluation of thermal resistance.

2.2.1. Selection of the Model Parameters

The bridge deck consists of concrete and separates the upper and lower traffic lanes. Because of symmetry, the domain has a length of half the bridge width, a width of 1 m, and a height equal to the thickness of the concrete slab. In regard to four-, six-, or eight-lane bridges, the bridge width is four, six, or eight times, respectively, the width of each motorway, namely, 3.75 m. Hence, the width of the model is 7.5, 11.25, or 15 m for the four-, six-, or eight-lane bridges, respectively. Generally, the length of a road bridge is very large, ranging from a few hundred meters to a few thousand meters. In this study, the unit length, i.e., that of a 1-m bridge deck unit, is directly selected as the research unit. The thickness of the concrete slab is set to 25 cm (data obtained from Bower). The centerline of the tubes is 6 cm below the deck surface (data obtained from the Chinese code for the design of concrete structures, GB 50010-2010), as shown in Figure 3. The tubes (cross-linked polyethylene (PEX) tubes) have an inner diameter of 2 cm and an outer diameter of 2.6 cm. Other parameters (e.g., tube spacing, inlet temperature, flow rate, ambient temperature, and wind speed) are presented below.

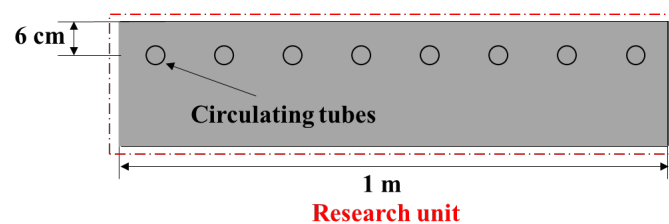


Figure 3. Schematic of the concrete cover and research unit (side view of the bridge deck).

Values of all the physical properties of the material summarized in Table 1 are retrieved from Zhang et al. [31].

Table 1. Physical properties of the material.

Property	Material	Value
Density (kg/m ³)	Concrete	2300
	Carrier Fluid	1000
	Air	1.23
Heat Capacity (J/(kg·K))	Concrete	880
	Carrier Fluid	3691
	Air	1006
Thermal Conductivity (W/(m·K))	Concrete	1.88
	Tube	0.41
	Carrier Fluid	0.61
	Air	0.0239
Surface Emissivity	Concrete	0.91
Dynamic Viscosity (kg/(m·s))	Carrier Fluid	0.00273
Kinematic Viscosity (m ² /s)	Air	1.315 × 10 ⁻⁵

2.2.2. Model Assumptions

The inlet temperature basically remains constant, and the flow rate of the circulating fluid in the tube is constant.

Due to the smaller volumetric mass, lower heat capacity and much higher thermal conductivity than those of concrete, rebar is not modeled. In addition, the relatively small rebar size requires a very fine mesh, which greatly increases the computation time. Moreover, according to the preliminary analysis performed by Bower et al. [24], the effect of rebar is negligible.

The ambient temperature is maintained constant, and snow melting is not included. This assumption is made to simplify the simulation process and, at the same time, can be regarded as the case whereby the bridge deck is preheated above the freezing temperature before snowfall. Therefore, if heat injection compensates for the heat demand during the melting process after snowfall, the bridge deck remains snow free after snowfall.

2.2.3. Initial and Boundary Conditions

At $t = 0$, the temperature of the concrete bridge deck and the fluid in the circulating tubes equals the ambient temperature, the flow rate in the tubes is the same as the inlet flow rate, and the pressure is equal to the atmospheric pressure, which is expressed as follows:

$$T_{concrete} = T_{amb}, \quad (1)$$

$$T_{tube} = T_{amb}, \quad (2)$$

$$u = v, \quad (3)$$

$$p = 1[atm], \quad (4)$$

where $T_{concrete}$ is the temperature of the concrete bridge deck, T_{tube} is the temperature of fluid in the circulating tubes, T_{amb} is the ambient temperature, u is the flow rate in the tubes, v is the flow rate at the inlet, and p is the pressure.

Due to symmetry, the two surfaces parallel to the circulating tubes, namely, the left and right surfaces, are considered adiabatic (i.e., the second boundary condition) and represented by the following:

$$-\vec{n} \cdot \vec{q} = 0, \quad (5)$$

where \vec{n} is the normal vector of the outer surface, and \vec{q} is the outward heat flux of the outer surface.

The upper, lower, front, and end faces of the model are in direct contact with air and exchange heat with the external air environment through convection, which are air convection surfaces represented by:

$$-\vec{n} \cdot \vec{q} = h(T_{ext} - T_{concrete}), \quad (6)$$

where T_{ext} is the external air temperature, and h is the convective heat transfer coefficient of the bridge deck surface, which is calculated as follows [32]:

$$h = \begin{cases} 2 \cdot \frac{k}{L} \cdot \frac{0.3387Pr^{1/3}Re_L^{1/2}}{(1 + (\frac{0.0468}{Pr})^{2/3})^{1/4}} & \text{if } Re_L \leq 5 \cdot 10^5 \\ 2 \cdot \frac{k}{L} \cdot Pr^{1/3} \cdot (0.037Re_L^{4/5} - 871) & \text{if } Re_L > 5 \cdot 10^5 \end{cases}, \quad (7)$$

where k is the thermal conductivity, L is the plate length, Pr is the Prandtl number, and Re_L is the Reynolds number, which is related to the fluid flow rate, namely, the wind speed in this study.

Concrete is not an absolute black body, namely, the upper, lower, front, and end faces of the model exchange radiation heat with surrounding objects and air, which is calculated as follows:

$$-\vec{n} \cdot \vec{q} = \varepsilon\sigma(T_{amb}^4 - T_{concrete}^4), \quad (8)$$

where ε is the surface emissivity and σ is the Boltzmann constant.

At the contact surface between the concrete bridge deck and circulating tubes, the temperatures of the circulating tubes and concrete are the same, which is represented by:

$$T_{concrete} = T_{tube}. \quad (9)$$

2.3. Model Validation and Preliminary Analysis

The proposed numerical model is verified against Zhang et al.'s [31] numerical simulations. Parametric analysis is performed to investigate the effects of several important parameters (i.e., tube spacing (S_t), inlet temperature (T_i), flow rate (v), and concrete cover (C_c)) on the heat transfer performance. The bridge deck is 3.5 m long, 0.4 m wide, and 0.25 m high. The baseline conditions are as follows: the tube spacing is 20 cm, the tube diameter is 2 cm, the heat transfer fluid inlet temperature is 12 °C, and the flow rate is 0.6 m/s. The ambient temperature is −2 °C, and the wind speed is 0. The material properties are consistent with those listed in Table 1.

A comparison of the average top surface temperature between the present study and the results of Zhang et al. [31] is shown in Figure 4, and an excellent agreement is observed. The results indicate that the average top surface temperature rapidly increases at the beginning of the simulation and gradually stabilizes after approximately 3 h. In addition, as shown in Figure 4a, the average top surface temperature decreases with increasing tube spacing. Figure 4b reveals that an increase in inlet fluid temperature will increase the surface temperature. As shown in Figure 4c, compared to the other factors, the flow rate imposes less influence on the surface temperature. Therefore, in the design of the subsequent optimization scheme, it is not recommended to enhance the system's snow melting capacity by increasing the flow rate. As shown in Figure 4d, an increase in concrete cover decreases the surface temperature because it directly affects the heat transfer distance of the heat source (i.e., the distance of heat transfer fluid to the bridge deck).

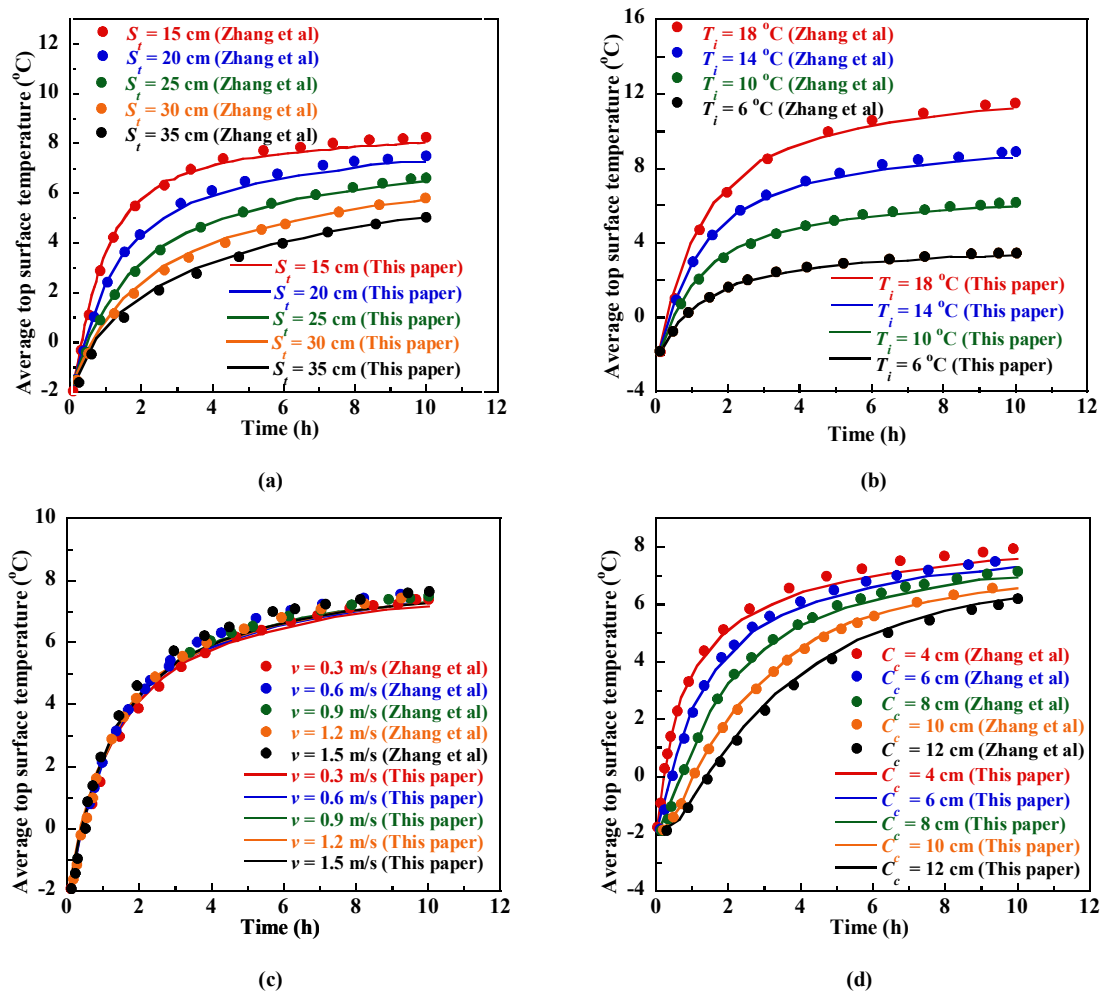


Figure 4. Comparison of the average top surface temperature between the present study and Zhang et al. [31] considering the (a) tube spacing, S_t ; (b) inlet temperature, T_i ; (c) flow rate, v ; and (d) concrete cover, C_c .

2.4. Evaluation Indexes

In the preliminary analysis in the previous chapter, the average top surface temperature is adopted to reflect the system's ability to melt snow and ice. Obviously, the higher the average top surface temperature is, the higher the snow melting capacity of the system is. However, this index is not comprehensive and does not consider economic and construction factors. Therefore, it is necessary to introduce other indicators to calibrate the snow melting effect.

2.4.1. Average Top Surface Temperature

The first index is the average top surface temperature, T_{ats} . The average top surface temperature intuitively assesses snow melting effects. However, it also has obvious disadvantages. First, this index only represents the overall average temperature of the top surface, and the temperature distribution of the top surface is obviously not uniform. Therefore, even if the average temperature is high, this does not indicate an overall good effect of snow melting on the top surface of the bridge deck. Second, the average temperature of the top surface only considers the temperature without considering other factors. In particular, the higher the top surface temperature is, the faster heat is dissipated and the worse the economic effect is. The average top surface temperature should be controlled as much as possible while ensuring the system's snow melting ability.

2.4.2. Snow Melting Proportion

The snow melting proportion, P_{sm} , represents the proportion of the effective snow melting area at the top of the bridge deck. When the temperature of the bridge deck ranges from 2~3 °C, the deicing effect is optimal, and in the preheated case, the snow melting proportion is determined as the proportion of the area at the top of the bridge deck where the temperature exceeds 3 °C. In the nonpreheated case, the snow melting proportion represents the proportion of the upper snow and ice that melts.

2.4.3. Heat Absorption Power

The inlet and outlet temperature difference, ΔT , is the difference between the outlet temperature, T_o , and the inlet temperature, T_i , when the heat transfer fluid flows through the heated bridge deck. The larger the inlet and outlet temperature difference is, the more heat is absorbed by the bridge deck and the higher the heat absorption power, P , of the heated bridge deck system is, which is calculated as follows:

$$P = \frac{c \cdot m \cdot \Delta T}{t} = c \cdot \frac{\rho \cdot V}{t} \cdot \Delta T = c \cdot \rho \cdot S \cdot v \cdot \Delta T, \quad (10)$$

where c is the specific heat capacity of the heat transfer fluid, ρ is the density of the heat transfer fluid, S is the area of the inner section of the tubes, and v is the flow rate.

2.4.4. Synthetic Evaluation Index

To comprehensively consider other factors, the synthetic evaluation index, Q , is defined and presented in the study. The synthetic evaluation index refers to the ratio of the product of the heat absorption power per unit tube length and the snow melting proportion to the corrected inflow temperature. Q is calculated as follows:

$$Q = \frac{P \cdot P_{sm}}{L \cdot (T_i - 1 \text{ } ^\circ\text{C})}, \quad (11)$$

where P/L is the heat absorption power per unit tube length, and the economic efficiency of tube consumption is considered in this part. $T_i - 1 \text{ } ^\circ\text{C}$ is the corrected inlet temperature, which represents the temperature increase of the ground source heat pump or energy foundation system over the heat transfer fluid temperature. As 1 °C is the lowest temperature of liquid water under atmospheric pressure, the corrected inflow temperature directly reflects the operating power of the ground source heat pump or energy foundation system. Obviously, the higher the inlet temperature is, the higher the operating power of the ground source heat pump or energy foundation system is and the higher the requirements are for the ground source heat pump or energy foundation system. The influence of the input power (inlet temperature) is considered in this part. Notably, the performance of snow melting cannot be blindly improved without considering the input power, and the input power (inlet temperature) should be reduced as much as possible under the premise of ensuring performance. During the subsequent optimization scheme selection process, the synthetic evaluation index, Q is mainly considered.

3. Results and Discussion

3.1. Layout of the Circulating Tubes

The heated bridge deck model is a bridge deck model with embedded circulating tubes. Liu et al. [20] emphasized that many pavement snow melting applications adopt the serpentine configuration. The layout forms of the circulating tubes vary, but the common layout can be divided into horizontal and vertical layouts, as shown in Figure 5.

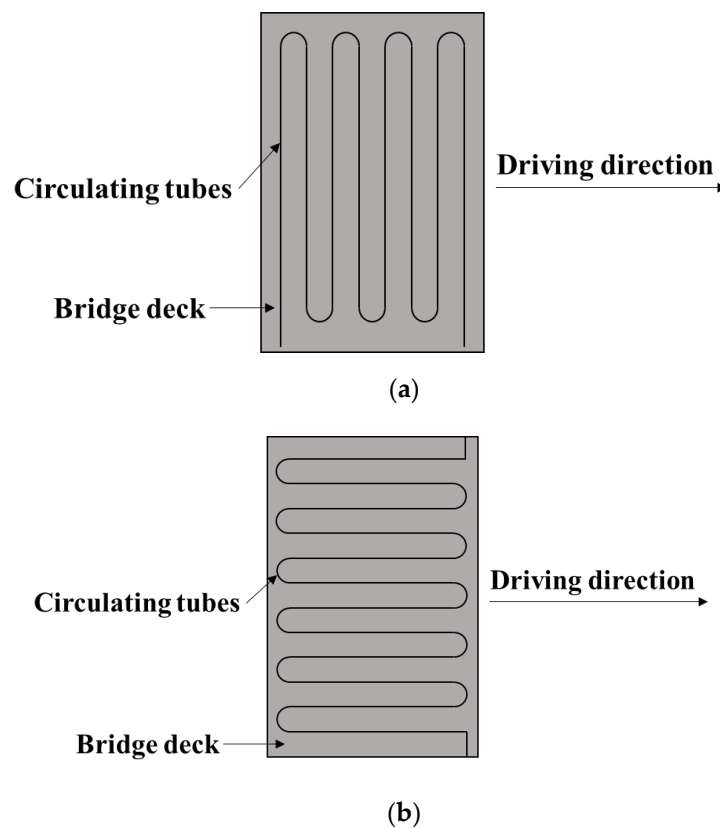


Figure 5. Schematic of the (a) horizontal layout and (b) vertical layout (plan view of the bridge deck).

To compare the snow melting effects of the above two layouts, four examples are selected in this study, and the relevant parameters are summarized in Table 2.

Table 2. Relevant parameters of the four examples.

Example	Tube Spacing, S_t (cm)	Inlet Temperature, T_i ($^{\circ}\text{C}$)
1	15	12
2	20	16
3	25	22
4	30	32

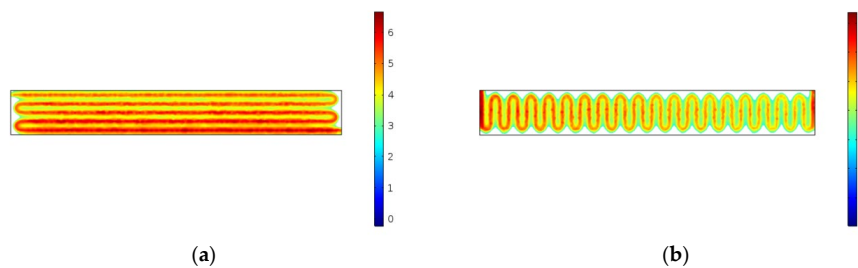
The established models are all based on the preheating operating condition, and the preheating time ranges from 3~4 h. In the model simulations, the results in the first 3~4 h are more important. Therefore, the outlet temperature, snow melting proportion, heat absorption power, and synthetic evaluation index are simulated and calculated at 3 h in this study. The results of each example are listed in Table 3.

According to Table 3, when the other parameters remain constant, the synthetic evaluation index of the horizontal layout is obviously higher than that of the vertical layout. Moreover, the horizontal layout is also better considering the snow melting proportion and heat absorption power. The horizontal layout is superior to the vertical layout in terms of snow melting ability, economic and energy saving considerations. Therefore, the horizontal layout is preferred in engineering practice.

Table 3. Results of the evaluation indexes for the four examples.

Example	Layout Forms	Tube Length, L (cm)	Outlet Temperature, T_o ($^{\circ}\text{C}$)	Snow Melting Proportion, P_{sm}	Heat Absorption Power, P (W)	Synthetic Evaluation Index, Q
1	Horizontal	5211.4	10.123	98.00%	1305.9	2.23
	Vertical	4684.5	10.253	84.60%	1215.45	2
2	Horizontal	3715.7	13.959	97.50%	1420	2.48
	Vertical	3482.4	14.128	79.30%	1302.42	1.98
3	Horizontal	2967.8	19.663	97.10%	1625.94	2.53
	Vertical	2688.8	19.938	75.70%	1434.61	1.92
4	Horizontal	2961.4	28.627	96.90%	2346.72	2.48
	Vertical	2191	29.549	73.80%	1705.25	1.85

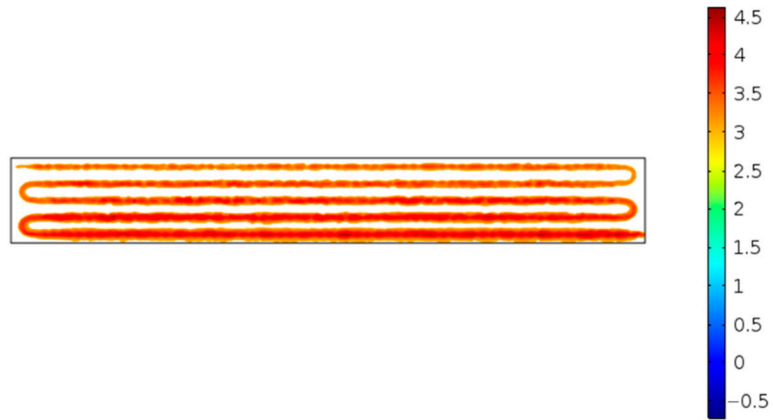
The above results demonstrate that the horizontal layout is better under the same conditions. To analyze the reasons for this result, the temperature distributions at the top of the heated bridge deck of example 2 under the horizontal and vertical layouts are shown in Figure 6 at 3 h. The bend of the tube is the part exhibiting the worst snow melting effect, and the temperature near these parts is almost below 3°C . Compared to the horizontal layout, the vertical layout contains more tube bends, and the snow melting effect of the vertical layout is thus not as good as that of the horizontal layout. Moreover, in the case of the horizontal layout, the tube bends are located on both sides of the driveway with a width only ranging from 10~20 cm. In practice, during driving, the wheels of vehicles hardly occur in this area. Therefore, it does not matter that the snow melting effect in the tube bend areas is poor. In regard to the vertical layout, the tube bends (i.e., the parts with a poor snow melting effect) are distributed along the two sides of the bridge deck unit. According to the symmetry, these areas widely occur on the bridge. Every meter, a bend area with a poor snow melting effect occurs on the bridge deck, which greatly affects the driving performance of vehicles. Based on the above considerations, the horizontal layout is the recommended layout of the circulating tubes.

**Figure 6.** Temperature distribution of the (a) horizontal layout and (b) vertical layout after 3 h of operation.

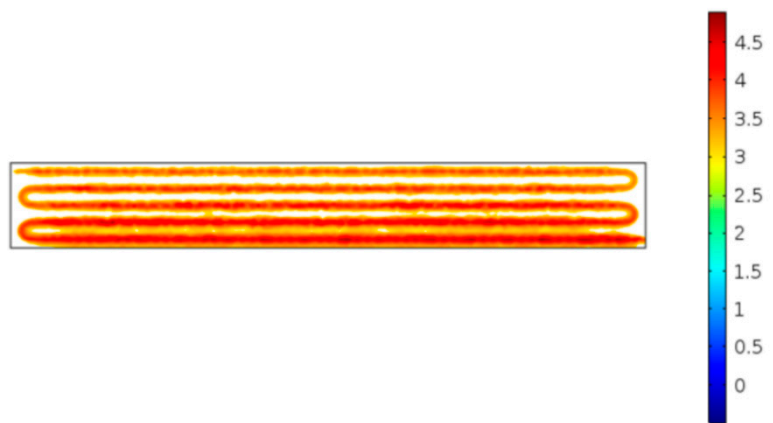
3.2. Optimal Design Scheme

Considering all of the above findings, the horizontal layout is the optimal layout. The subsequent studies will be based on the horizontal layout and will determine the optimal combination of the other parameters (i.e., the number of lanes, tube spacing, inlet temperature, and ambient temperature). Here, the snow melting proportion is adopted as an index to measure the snow melting effect. Figure 7 shows the temperature distribution at the top of the bridge deck at the different snow melting proportions (i.e., 50%, 70%, 90%, 95%, and 99%). Figure 7d reveals that at a snow melting proportion higher than 95%, the central part of the bridge deck is the effective snowmelt area, and poor areas only occur along both sides. The snow on either side does not affect the driving performance of vehicles. To study the optimal inlet temperature under the different tube spacings, the inlet temperature should be reduced as much as possible while still meeting the snow melting requirements. A decrease in the inlet temperature not only reduces the operating power of the ground source heat pump or energy foundation system, but also avoids the energy dissipation due to the high temperature at the top of the bridge deck and the excessive heat inside the bridge deck. Therefore, under a certain tube spacing, the lowest inlet temperature

at which a snow melting proportion of 95% is reached after 3 h of operation is defined as the optimal inlet temperature.



(a)



(b)



(c)

Figure 7. Cont.



(d)



(e)

Figure 7. Temperature distribution at the top of the bridge deck at the different snow melting proportions: (a) 50%, (b) 70%, (c) 90%, (d) 95%, (e) 99%.

3.2.1. Four-Lane Bridge

At an ambient temperature of $-2\text{ }^{\circ}\text{C}$, the simulation and calculation results under each tube spacing (i.e., 15, 20, 25, 30, and 35 cm) at the different inlet temperatures are summarized in Table 4.

In regard to the snow melting proportion, different fill colors are employed. Cyan indicates that the snow melting requirements are fully met (i.e., $P_{sm} > 95\%$), and yellow indicates that the snow melting effect is normal (i.e., $80\% < P_{sm} < 95\%$), while red indicates that the snow melting effect is poor (i.e., $P_{sm} < 80\%$). Under a certain tube spacing, the row of the optimal inlet temperature, T_{oi} , is marked in red, and the selection basis is the lowest inlet temperature at which a snow melting proportion of 95% is attained at 3 h.

Table 4. Results of the evaluation indexes under the different tube spacings, S_t , and inlet temperatures, T_i , after 3 h of operation (at an ambient temperature of $-2\text{ }^\circ\text{C}$).

Tube Spacing, S_t (cm)	Tube Length, L (cm)	Inlet Temperature, T_i ($^\circ\text{C}$)	Outlet Temperature, T_o ($^\circ\text{C}$)	Average Top Surface Temperature, T_{ats} ($^\circ\text{C}$)	Snow Melting Proportion, P_{sm}
15	5211.4	8	6.66	2.68	18.3%
	5211.4	10	8.39	3.61	93.8%
	5211.4	12	10.12	4.53	98.0%
	5211.4	14	11.85	5.46	98.8%
	5211.4	16	13.58	6.39	99.3%
20	3715.7	12	10.41	3.18	61.0%
	3715.7	14	12.19	3.92	95.5%
	3715.7	16	13.96	4.66	97.5%
	3715.7	18	15.73	5.39	97.9%
	3715.7	20	17.5	6.12	98.4%
	3715.7	22	19.28	6.86	98.7%
25	2967.8	18	16.05	4.15	79.6%
	2967.8	20	17.86	4.77	95.6%
	2967.8	22	19.66	5.38	97.1%
	2967.8	24	21.47	5.99	97.6%
	2967.8	26	23.27	6.61	97.8%
	2967.8	28	25.08	7.21	98.1%
30	2961.4	24	21.42	4.65	70.3%
	2961.4	26	23.22	5.16	80.4%
	2961.4	28	25.03	5.66	91.3%
	2961.4	30	26.83	6.17	96.3%
	2961.4	32	28.63	6.68	96.9%
	2961.4	34	30.43	7.18	97.2%
	2961.4	36	32.23	7.7	97.4%
	2961.4	38	34.03	8.19	97.5%
35	2220	40	36.8	7.84	93.8%
	2220	42	38.65	8.3	96.8%
	2220	44	40.5	8.78	97.1%

After choosing the optimal inlet temperature, the optimal tube spacing should be selected based on the synthetic evaluation index, Q . Detailed results of the five sets of optimal inlet temperatures under the corresponding tube spacings (marked in red in Table 4) are provided in Table 5. According to the synthetic evaluation index, at an ambient temperature of $-2\text{ }^\circ\text{C}$, the optimal tube spacing is 25 cm and the corresponding optimal inlet temperature is $20\text{ }^\circ\text{C}$.

Table 5. Detailed results of the evaluation indexes for the five combinations of the tube spacing S_t and optimal inlet temperature T_{oi} (at an ambient temperature of $-2\text{ }^\circ\text{C}$).

Tube Spacing, S_t (cm)	Tube Length, L (cm)	Optimal Inlet Temperature, T_{oi} ($^\circ\text{C}$)	Outlet Temperature, T_o ($^\circ\text{C}$)	Snow Melting Proportion, P_{sm}	Heat Absorption Power, P (W)	Synthetic Evaluation index, Q
15	5211.4	12	10.12	98.0%	1305.9	2.23
20	3715.7	14	12.19	95.5%	1262.07	2.49
25	2967.8	20	17.86	95.6%	1490.27	2.53
30	2961.4	30	26.83	96.3%	2208.27	2.48
35	2220	42	38.65	96.8%	2332.81	2.48

When the ambient temperature is -4 , -6 , -8 , or $-10\text{ }^\circ\text{C}$, the optimal inlet temperature can be obtained using a similar approach to the previous method. The results are shown in Figure 8.

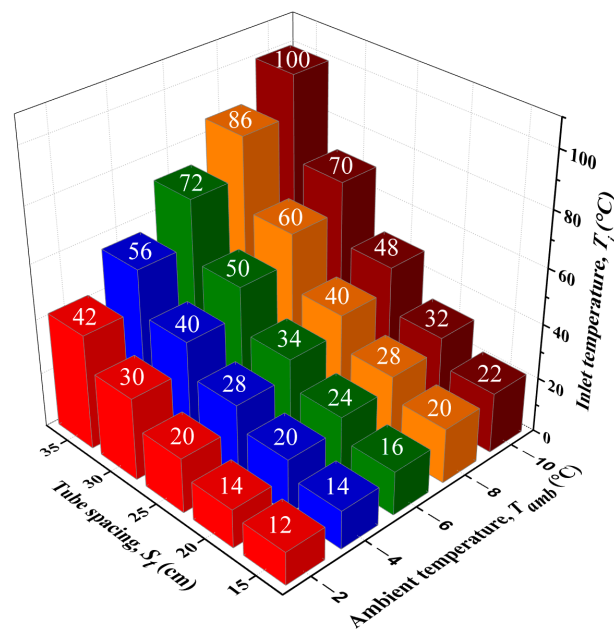


Figure 8. Optimal inlet temperature, T_{oi} , under the different tube spacings, S_t , and ambient temperatures, T_{amb} (four-lane bridge).

According to Figure 8, an empirical equation of the optimal inlet temperature with the ambient temperature is obtained by linear fitting as follows:

$$T_{oi} = \begin{cases} -1.3T_{amb} + 9 & \text{when } S_t = 15 \text{ cm} \\ -2.2T_{amb} + 10.4 & \text{when } S_t = 20 \text{ cm} \\ -3.4T_{amb} + 13.6 & \text{when } S_t = 25 \text{ cm} \\ -5T_{amb} + 20 & \text{when } S_t = 30 \text{ cm} \\ -7.3T_{amb} + 27.4 & \text{when } S_t = 35 \text{ cm} \end{cases} . \quad (12)$$

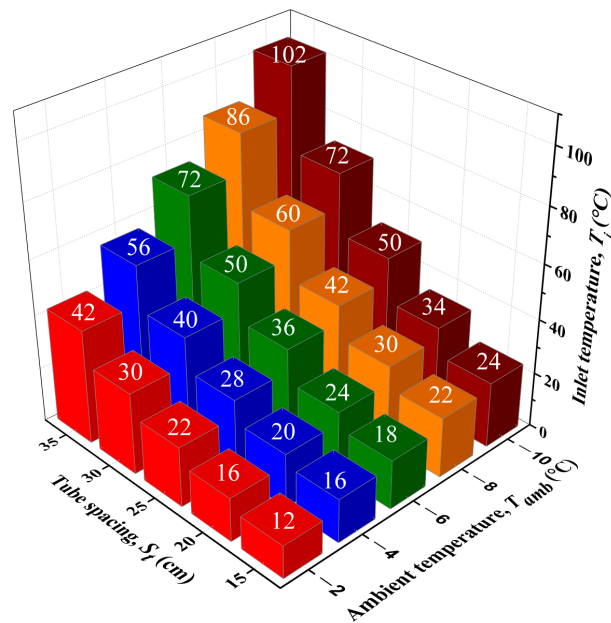
In addition, an empirical equation of the optimal inlet temperature with the tube spacing is obtained by quadratic function fitting as follows:

$$T_{oi} = \begin{cases} 0.0686S_t^2 - 1.9086S_t + 25.029 & \text{when } T_{amb} = -2 \text{ }^\circ\text{C} \\ 0.0686S_t^2 - 1.3486S_t + 19.029 & \text{when } T_{amb} = -4 \text{ }^\circ\text{C} \\ 0.0971S_t^2 - 2.0971S_t + 26.057 & \text{when } T_{amb} = -6 \text{ }^\circ\text{C} \\ 0.1257S_t^2 - 3.0057S_t + 37.086 & \text{when } T_{amb} = -8 \text{ }^\circ\text{C} \\ 0.1314S_t^2 - 2.6914S_t + 32.971 & \text{when } T_{amb} = -10 \text{ }^\circ\text{C} \end{cases} . \quad (13)$$

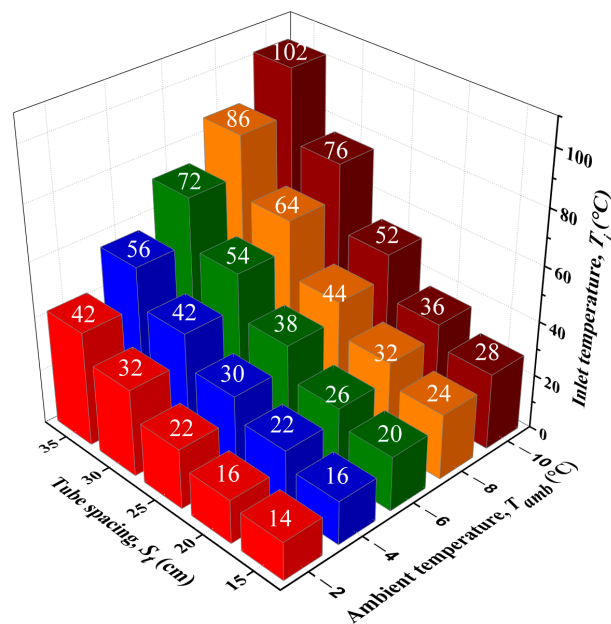
The above two empirical equations predict the optimal inlet temperature of a four-lane heated bridge deck system with the ambient temperature ranging from approximately -2 to -10 $^\circ\text{C}$ and the tube spacing ranging from 15 – 35 cm under the preheated operation mode.

3.2.2. Six-Lane and Eight-Lane Bridges

Following a method similar to that applied to four-lane bridges, we obtain the optimal inlet temperature for six-lane and eight-lane bridges. The process is omitted for brevity, and the results are shown in Figure 9.



(a)



(b)

Figure 9. Optimal inlet temperature, T_{oi} , under the different tube spacings, S_t , and ambient temperatures, T_{amb} , for (a) a six-lane bridge and (b) an eight-lane bridge.

Similarly, empirical equations are obtained by linear fitting and quadratic function fitting, respectively, as follows:

For a six-lane bridge:

$$T_{oi} = \begin{cases} -1.5T_{amb} + 9.4 & \text{when } S_t = 15 \text{ cm} \\ -2.3T_{amb} + 11 & \text{when } S_t = 20 \text{ cm} \\ -3.5T_{amb} + 14.6 & \text{when } S_t = 25 \text{ cm} \\ -5.2T_{amb} + 19.2 & \text{when } S_t = 30 \text{ cm} \\ -7.5T_{amb} + 26.6 & \text{when } S_t = 35 \text{ cm} \end{cases}, \quad (14)$$

$$T_{oi} = \begin{cases} 0.0514S_t^2 - 1.0914S_t + 16.971 & \text{when } T_{amb} = -2\text{ }^\circ\text{C} \\ 0.08S_t^2 - 2S_t + 28 & \text{when } T_{amb} = -4\text{ }^\circ\text{C} \\ 0.0971S_t^2 - 2.1771S_t + 28.857 & \text{when } T_{amb} = -6\text{ }^\circ\text{C} \\ 0.12S_t^2 - 2.84S_t + 38 & \text{when } T_{amb} = -8\text{ }^\circ\text{C} \\ 0.1314S_t^2 - 2.6914S_t + 34.971 & \text{when } T_{amb} = -10\text{ }^\circ\text{C} \end{cases} \quad (15)$$

For an eight-lane bridge:

$$T_{oi} = \begin{cases} -1.8T_{amb} + 9.6 & \text{when } S_t = 15\text{ cm} \\ -2.5T_{amb} + 11.4 & \text{when } S_t = 20\text{ cm} \\ -3.7T_{amb} + 15 & \text{when } S_t = 25\text{ cm} \\ -5.5T_{amb} + 20.6 & \text{when } S_t = 30\text{ cm} \\ -7.5T_{amb} + 26.6 & \text{when } S_t = 35\text{ cm} \end{cases} \quad (16)$$

$$T_{oi} = \begin{cases} 0.0571S_t^2 - 1.4171S_t + 22.057 & \text{when } T_{amb} = -2\text{ }^\circ\text{C} \\ 0.0571S_t^2 - 0.8571S_t + 16.057 & \text{when } T_{amb} = -4\text{ }^\circ\text{C} \\ 0.08S_t^2 - 1.36S_t + 22 & \text{when } T_{amb} = -6\text{ }^\circ\text{C} \\ 0.1029S_t^2 - 2.0229S_t + 31.143 & \text{when } T_{amb} = -8\text{ }^\circ\text{C} \\ 0.1257S_t^2 - 2.5257S_t + 37.086 & \text{when } T_{amb} = -10\text{ }^\circ\text{C} \end{cases} \quad (17)$$

With the use of the same method as that described in the previous section, the optimal scheme under the different conditions is determined. When designing a heated bridge deck, we can determine the optimal tube spacing and corresponding inlet temperature according to local weather data (ambient temperature) and the number of bridge lanes in combination with Table 6 below.

Table 6. Optimal combination of the tube spacing, S_t , and inlet temperature, T_{oi} , under the different combinations of the number of lanes and ambient temperature, T_{amb} .

Ambient Temperature		-2 °C	-4 °C	-6 °C	-8 °C	-10 °C
Number of Lanes						
4		25 cm/	25 cm/	20 cm/	20 cm/	20 cm/
		20 °C	28 °C	24 °C	28 °C	32 °C
6		25 cm/	25 cm/	25 cm/	20 cm/	20 cm/
		22 °C	28 °C	36 °C	30 °C	34 °C
8		25 cm/	25 cm/	25 cm/	25 cm/	25 cm/
		22 °C	30 °C	38 °C	44 °C	52 °C

3.3. Further Discussion and Optimization of the Design Scheme

In this part, the snow melting effect of the optimal design scheme determined in Section 3.2 at the different wind speeds is studied, and corresponding adjustment methods are proposed. Several optimization schemes for the design of a heated bridge deck are then proposed and examined.

3.3.1. Influence of the Wind Speed

When studying the influence of the wind speed, v_w , the selected research scheme is among the optimal six-lane bridge deck design schemes at -2 °C, under a tube spacing of 20 cm, and the inlet temperature is 16 °C.

Figure 10 shows the variation in the snow melting proportion over time at the different wind speeds (i.e., 0, 1, 2, 4, and 6 m/s). As shown in Figure 10, the higher the wind speed is, the slower the snow melting proportion rises. When the wind speed is lower than or equal to 2 m/s, the snow melting proportion reaches 95% after the system is operated for 4 h, which satisfies the snow melting requirements. At a wind speed higher than 2 m/s, the snow melting requirements are not met, and the inlet temperature should be appropriately increased to satisfy the functional requirements.

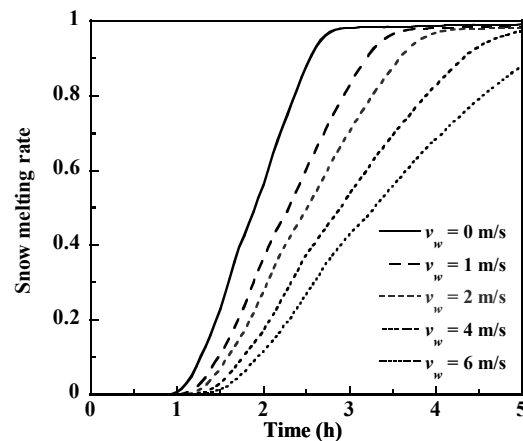


Figure 10. Snow melting proportion, P_{sm} , variation at the different wind speeds, v_w .

Based on the above analysis, the heated bridge deck designed according to the optimal design scheme analyzed in Section 3.2 may still meet the melting snow requirements where the wind speed does not exceed 2 m/s, but the preheating time should be extended by 1 h, namely, the preheating time should be set to 4 h.

3.3.2. Addition of a Heat Insulation Layer at the Bottom of the Bridge Deck

Since the bottom surface of a heated bridge deck functions as an air convection surface, the heat transferred from the circulation tubes to the bottom surface is carried away by air and dissipated, which does not facilitate energy reduction. Therefore, measures should be implemented to transfer more heat to the top surface of the bridge deck, and an insulation layer is considered at the bottom of the bridge deck.

When studying the influence of an insulation layer, the selected research scheme is one of the optimal four-lane bridge deck design schemes at -10 °C. Moreover, the tube spacing is 20 cm, the inlet temperature is 32 °C, and the wind speed is 0 m/s.

Figure 11 shows the variation in the snow melting proportion variation over time without and with an insulation layer. As shown in Figure 11, the two increasing curves of the snow melting proportion basically coincide. Figure 12 shows the isotherm contours in the middle section of the bridge deck without and with an insulation layer after 3 h of operation. Comparing the two cases, the temperature distributions in the two cases are almost the same, i.e., the presence or absence of the heat insulation layer imposes little effect on the temperature distribution in the middle section of the bridge deck. At the end of 3 h, the average top surface temperature without an insulation layer is 5.63 °C, and the average top surface temperature with an insulation layer is 5.64 °C. The increase in the average top surface temperature due to the insulation layer is also minimal. When no insulation layer occurs at the bottom of the bridge deck, the temperature of the lower part of the bridge deck is very low because the circulating tubes are close to the top of the bridge deck, and the temperature of the bottom surface is almost equal to the ambient temperature. The heat flux at the bottom of the bridge deck is almost zero, which is equivalent to having an insulation layer. Therefore, there is no need to add a heat insulation layer at the bottom of the bridge deck.

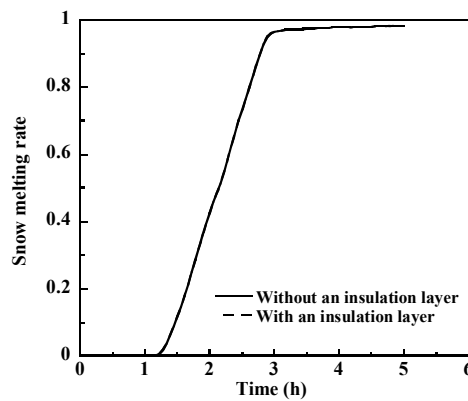


Figure 11. Snow melting proportion P_{sm} variation with and without an insulation layer.

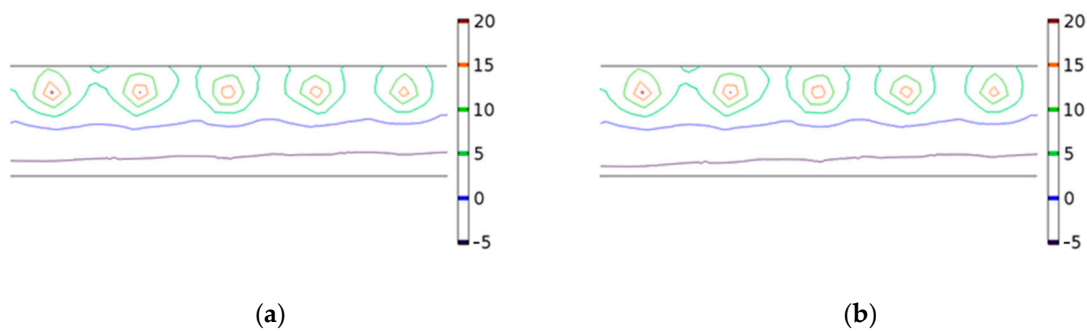


Figure 12. Isotherm contours in the middle section of the bridge deck (a) without and (b) with an insulation layer after 3 h of operation.

3.3.3. Only Arranging Tubes near the Wheels

In the design of a heated bridge deck system, there are two forms for the layout area of the circulating tubes: one approach is to cover the entire bridge deck area with the circulating tubes, which is suitable in areas with a high traffic volume; the other approach is to only arrange circulating tubes at the wheels. This method is suitable in areas with a low traffic volume. From the perspective of energy savings, it is obvious that the second method is more energy efficient.

The width of a vehicle is generally 2.5 m, and the wheel spacing is 1.8 m (data obtained from the Chinese technical standard of highway engineering, JTG B01-2014). Considering that a vehicle may slightly shift left or right during driving and that the wheel spacing of various vehicles is slightly different, the width of the circulating tube area near each wheel is set to 0.6 m, as shown in Figure 13.

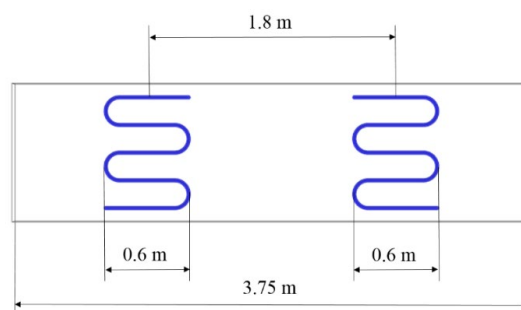


Figure 13. Schematic of the tube arrangement only near the wheels.

Single-lane simulations are performed. The relevant parameters of the model are as defined follows: the circulation tube spacing is 20 cm, the inflow temperature is 32 °C, the ambient temperature is −10 °C, and the wind speed is 0 m/s.

Figure 14 shows the temperature distribution at the top of the bridge deck under the two layouts after 3 h of operation. As shown in Figure 14b, at the end of 3 h, the temperature in the wheel area is basically higher than 3 °C. When snowfall occurs, this may ensure that no snow accumulation occurs in this area, which may still meet the functional requirements of heating the bridge deck. Therefore, in areas with a low traffic volume, it is better to only arrange tubes near the wheels in a given lane in terms of the economy.

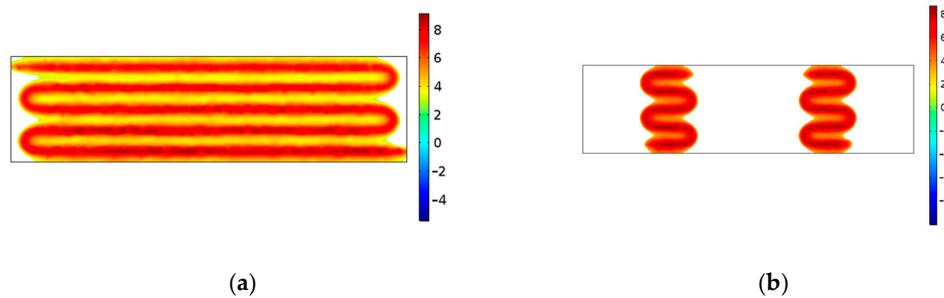


Figure 14. Temperature distribution at the top of the bridge deck after 3 h of operation (a) by covering the entire bridge deck area with tubes and (b) only arranging tubes near wheels.

4. Conclusions

COMSOL Multiphysics finite element software is adopted for simulation purposes in this study. First, a geothermally heated bridge deck is introduced as an example to study geothermally heated systems. Second, a preliminary parametric analysis is performed to investigate the effects of several important parameters (i.e., tube spacing (S_t), inlet temperature (T_i), flow rate (v), and concrete cover (C_c)) on the heat transfer performance, and the results are compared and validated. Third, three evaluation indexes (i.e., average top surface temperature (T_{ats}), snow melting proportion (P_{sm}), and heat absorption power (P)) are described, and a synthetic evaluation index (Q) is then defined and proposed to comprehensively consider the above influencing factors. Subsequently, mainly referring to the synthetic evaluation index, the optimal design scheme of the geothermally heated bridge deck system under various conditions (i.e., circulating tube layout, lane number, ambient temperature (T_{amb}), and tube spacing (S_t)) is determined and analyzed to calculate the optimal inlet temperature (T_{oi}) and guide the design of heated bridge decks. Finally, the influence of the wind speed and two adjustment methods (i.e., the addition of a heat insulation layer at the bottom of the bridge deck and only arranging tubes near wheels) is studied.

The main conclusions of the present work are as follows:

- (1) T_{ats} decreases with increasing S_t and T_i . Compared to the other factors, v exerts less influence on T_{ats} . Therefore, it is not recommended to enhance the system's snow melting capacity by increasing v . An increase in C_c may decrease T_{ats} because this directly affects the heat transfer distance of the heat source.
- (2) The tube bend area is the part with the worst snow melting effect, and the temperature in these parts is almost below 3 °C. Every meter, a tube bend occurs on the bridge deck with a poor snow melting effect under the vertical layout, which greatly impairs the driving performance of vehicles.
- (3) When the other parameters remain unchanged, the Q value under the horizontal layout is obviously higher than that under the vertical layout. Moreover, the horizontal layout is also better considering P_{sm} and P . The horizontal layout is the recommended layout of the circulating tubes.
- (4) Referring to Q , the optimal design scheme of the geothermally heated bridge deck system under the different lane numbers and conditions is determined. The obtained empirical equations show that T_{oi} varies linearly with T_{amb} and exhibits a quadratic function relationship with S_t .

- (5) The optimally designed heated bridge deck may still satisfy the snow melting requirements at a wind speed not higher than 2 m/s, but the preheating time should be extended by 1 h. The increasing curves of the snow melting proportion without and with an insulation layer basically coincide, and thus, there is no need to add a heat insulation layer at the bottom of the bridge deck. In areas with a low traffic volume, it is better to only arrange tubes near the wheels in a given lane in terms of the economic considerations.

Author Contributions: Conceptualization, H.P. and J.C.; methodology, W.L. and J.C.; software, W.L. and Z.G.; formal analysis, W.L. and Z.G.; writing—original draft preparation, W.L.; writing—review and editing, H.P. and J.C.; supervision, H.P. and J.C. All authors have read and agreed to the published version of the manuscript.

Funding: This research was funded by the Major Technological Innovation Projects of Hubei (No. 2018AAA028 and No. 2017AAA128).

Conflicts of Interest: The authors declare no conflict of interest.

References

1. Ho, I.-H.; Dickson, M. Numerical modeling of heat production using geothermal energy for a snow-melting system. *Géoméch. Energy Environ.* **2017**, *10*, 42–51. [[CrossRef](#)]
2. Mensah, K.; Choi, J.M. Review of technologies for snow melting systems. *J. Mech. Sci. Technol.* **2015**, *29*, 5507–5521. [[CrossRef](#)]
3. Mirzananadi, R.; Hagentoft, C.-E.; Johansson, P.; Johnsson, J. Anti-icing of road surfaces using Hydronic Heating Pavement with low temperature. *Cold Reg. Sci. Technol.* **2018**, *145*, 106–118. [[CrossRef](#)]
4. Liu, X.; Rees, S.J.; Spitler, J.D. Modeling snow melting on heated pavement surfaces. Part I: Model development. *Appl. Therm. Eng.* **2007**, *27*, 1115–1124. [[CrossRef](#)]
5. Hassan, Y.; Abd El Halim, A.O.; Razaqpur, A.G.; Bekheet, W.; Farha, M.H. Effects of Runway Deicers on Pavement Materials and Mixes: Comparison with Road Salt. *J. Transp. Eng.* **2002**, *128*, 385–391. [[CrossRef](#)]
6. Fay, L.; Shi, X. Environmental Impacts of Chemicals for Snow and Ice Control: State of the Knowledge. *Water Air Soil Pollut.* **2012**, *223*, 2751–2770. [[CrossRef](#)]
7. Zhao, H.; Wu, Z.; Wang, S.; Zheng, J.; Che, G. Concrete pavement deicing with carbon fiber heating wires. *Cold Reg. Sci. Technol.* **2011**, *65*, 413–420. [[CrossRef](#)]
8. Maleki, P.; Iranpour, B.; Shafabakhsh, G. Investigation of de-icing of roads with conductive concrete pavement containing carbon fibre-reinforced polymer (CFRP). *Int. J. Pavement Eng.* **2017**, *20*, 682–690. [[CrossRef](#)]
9. Liu, Y.; Lai, Y.; Ma, D.X. Melting snow on airport cement concrete pavement with carbon fibre heating wires. *Mater. Res. Innov.* **2015**, *19*, S10–S95. [[CrossRef](#)]
10. Liu, K.; Huang, S.; Jin, C.; Xie, H.; Wang, F. Prediction models of the thermal field on ice-snow melting pavement with electric heating pipes. *Appl. Therm. Eng.* **2017**, *120*, 269–276. [[CrossRef](#)]
11. Lai, Y.; Liu, Y.; Su, X.; Ma, D.X.; Wang, P. The influence of heat flux on melting ice on concrete pavement with carbon fibre heating wire. *IOP Conf. Ser. Mater. Sci. Eng.* **2018**, *392*, 022021. [[CrossRef](#)]
12. Noguchi, T.; Sakurada, K.; Tsukidate, T. Housing design in the snowy regions in Japan- incase of Hokkaido. In Proceedings of the Fifth International Conference on Snow Engineering, Davos, Switzerland, 5–8 July 2004; pp. 47–52.
13. Sivasakthivel, T.; Murugesan, K.; Sahoo, P.K. A study on energy and CO₂ saving potential of ground source heat pump system in India. *Renew. Sustain. Energy Rev.* **2014**, *32*, 278–293. [[CrossRef](#)]
14. Wang, H.; Liu, L.; Chen, Z. Experimental investigation of hydronic snow melting process on the inclined pavement. *Cold Reg. Sci. Technol.* **2010**, *63*, 44–49. [[CrossRef](#)]
15. Spitler, J.D.; Ramamoorthy, M. Bridge deck deicing using geothermal heat pumps. In Proceedings of the Fourth International Heat Pumps in Cold Climates Conference, Aylmer, QC, Canada, 17–18 August 2000; pp. 1–16.
16. Ho, I.H.; Li, S.; Abudureyimu, S. Alternative hydronic pavement heating system using deep direct use of geothermal hot water. *Cold Reg. Sci. Technol.* **2019**, *160*, 194–208. [[CrossRef](#)]
17. Yehia, S.A.; Tuan, C.Y. Airfield Pavement Deicing with Conductive Concrete Overlay. In Proceedings of the Federal Aviation Administration Technology Transfer Conference, Atlantic City, NJ, USA, 5–7 May 2002.

18. Chen, M.; Wu, S.; Wang, H.; Zhang, J. Study of ice and snow melting process on conductive asphalt solar collector. *Sol. Energy Mater. Sol. Cells* **2011**, *95*, 3241–3250. [[CrossRef](#)]
19. Pan, P.; Wu, S.; Xiao, Y.; Liu, G. A review on hydronic asphalt pavement for energy harvesting and snow melting. *Renew. Sustain. Energy Rev.* **2015**, *48*, 624–634. [[CrossRef](#)]
20. Liu, X. Development and Experimental Validation of Simulation of Hydronic Snow Melting Systems for Bridges. Ph.D. Thesis, Tongji University, Shanghai, China, 1998.
21. Liu, X.; Rees, S.J.; Spitler, J.D. Modeling snow melting on heated pavement surfaces. Part II: Experimental validation. *Appl. Therm. Eng.* **2007**, *27*, 1125–1131. [[CrossRef](#)]
22. Wang, H.; Chen, Z. Study of critical free-area ratio during the snow-melting process on pavement using low-temperature heating fluids. *Energy Convers. Manag.* **2009**, *50*, 157–165. [[CrossRef](#)]
23. Olgun, C.G.; McCartney, J.S. Outcomes from international workshop on thermoactive geotechnical systems for near-surface geothermal energy: From research to practice. *DFI J. J. Deep. Found. Inst.* **2014**, *8*, 59–73. [[CrossRef](#)]
24. Bowers, G.A.; Olgun, C.G. Ground-Source Bridge Deck Deicing Systems Using Energy Foundations. Geo-characterization and Modeling for Sustainability. In Proceedings of the Geo Congress, Atlanta, GA, USA, 23–26 February 2014; pp. 2705–2714. [[CrossRef](#)]
25. Chiasson, A.D.; Spitler, J.D.; Rees, S.J.; Smith, M.D. A Model for Simulating the Performance of a Pavement Heating System as a Supplemental Heat Rejecter with Closed-Loop Ground-Source Heat Pump Systems. *J. Sol. Energy Eng.* **2000**, *122*, 183–191. [[CrossRef](#)]
26. Maya, S.M.; García-Gil, A.; Schneider, E.G.; Moreno, M.M.; Epting, J.; Vázquez-Suñé, E.; Marazuela, M.A.; Sánchez-Navarro, J.A. An upscaling procedure for the optimal implementation of open-loop geothermal energy systems into hydrogeological models. *J. Hydrol.* **2018**, *563*, 155–166. [[CrossRef](#)]
27. García-Gil, A.; Moreno, M.M.; Schneider, E.G.; Marazuela, M.A.; Abesser, C.; Lázaro, J.M.; Navarro, J.A.S. Nested shallow geothermal systems. *Sustainability* **2020**, *12*, 5152. [[CrossRef](#)]
28. García-Gil, A.; Abesser, C.; Cavero, S.G.; Marazuela, M.A.; Lázaro, J.M.; Vázquez-Suñé, E.; Hughes, A.G.; Moreno, M.M. Defining the exploitation patterns of groundwater heat pump systems. *Sci. Total Environ.* **2020**, *710*, 136425. [[CrossRef](#)] [[PubMed](#)]
29. Bowers, G.A. Ground-Source Bridge Deck Deicing and Integrated Shallow Geothermal Energy Harvesting Systems. Ph.D. Thesis, Virginia Polytechnic Institute and State University, Blacksburg, VA, USA, 2016.
30. COMSOL Multiphysics® v. 5.3. COMSOL AB, Stockholm, Sweden. Available online: www.comsol.com (accessed on 15 December 2020).
31. Zhang, N.; Yu, X.; Li, T. Numerical Simulation of Geothermal Heated Bridge Deck. In Proceedings of the International Conference on Transportation Infrastructure and Materials, Qingdao, China, 9–12 June 2017.
32. Incropera, F.P.; DeWitt, D.P.; Bergman, T.L.; Lavine, A.S. *Fundamentals of Heat and Mass Transfer*, 6th ed.; John Wiley & Sons: Hoboken, NJ, USA, 2006.

Publisher’s Note: MDPI stays neutral with regard to jurisdictional claims in published maps and institutional affiliations.



© 2020 by the authors. Licensee MDPI, Basel, Switzerland. This article is an open access article distributed under the terms and conditions of the Creative Commons Attribution (CC BY) license (<http://creativecommons.org/licenses/by/4.0/>).